Argonne NATIONAL LABORATORY

ANL/ESIA-22/3

Electrolyzers for Hydrogen Production: Solid Oxide, Alkaline, and Proton Exchange Membrane

Energy Systems and Infrastructure Analysis Division

ANL/ESIA-22/3

Electrolyzers for Hydrogen Production: Solid Oxide, Alkaline, and Proton Exchange Membrane

by
Rakesh Krishnamoorthy Iyer, Jarod C. Kelly, and Amgad Elgowainy
Energy Systems and Infrastructure Analysis Division, Argonne National Laboratory

October 2022

CONTENTS

FIGURE

TABLES

ACKNOWLEDGMENTS

This activity was supported by the Hydrogen and Fuel Cell Technologies Office (HFTO), Office of Energy Efficiency and Renewable Energy, United States Department of Energy under Contract Number DE-AC02-06CH11357. The authors would like to thank Neha Rustagi of HFTO for her guidance and support. The authors would also like to thank Cassidy Houchins, Jacob Prosser, Jennie Huya-Kouadio, and Kevin McNamara from Strategic Analysis Inc., for providing valuable data and inputs on the electrolyzers inventory (bill-of-materials) for all electrolyzers covered in this report. The views and opinions of the authors expressed herein do not necessarily state or reflect those of the U.S. Government or any agency thereof. Neither the U.S. Government nor any agency thereof, nor any of their employees, makes any warranty, expressed or implied, or assumes any legal liability or responsibility for the accuracy, completeness, or usefulness of any information, apparatus, product, or process disclosed, or represents that its use would not infringe privately owned rights.

ACRONYMS

AC	Alternating Current
AE	Alkaline Electrolysis
AEC	Alkaline Electrolysis Cell
BOM	Bill of Materials
BOP	Balance of Plant
CAPEX	Capital Expenditure
CeO_2	Cerium Dioxide (also called Ceria)
CH_2Cl_2	Dichloromethane
CH_4	Methane
Cl_2	Chlorine
CO_2	Carbon Dioxide
DC	Direct Current
DEA	Diaphragm Electrode Assembly
DI	De-ionized
EPDM	Ethylene Propylene Diene Monomer
FCEV	Fuel-Cell Electric Vehicle
GDC	Gadolinium-Doped Ceria
GDL	Gas Diffusion Layer
GHG	Greenhouse Gas
GREET	Greenhouse gases, Regulated Emissions, and Energy use in Transportation
GWP	Global Warming Potential
H^+	Hydrogen Ion
H_2	Hydrogen
H_2O	Water
HCl	Hydrochloric Acid
HDPE	High-Density Polyethylene
HER	Hydrogen Evolution Reaction
IR	Ionizing Radiation
KOH	Potassium Hydroxide
LCA	Life-Cycle Analysis
LCI	Life-Cycle Inventory
LSC	Lanthanum Strontium Chromite
LSCF	Lanthanum Strontium Cobalt Ferrite

MEA	Membrane Electrode Assembly
MMO	Mixed Metal Oxide
Mn	Manganese
$MnCO_3$	Manganese Carbonate
$MnSO_4$	Manganese Sulfate
Mo	Molybdenum
MW	Megawatt(s)
Na_2CO_3	Sodium Carbonate, or Soda Ash
$NaHCO_3$	Sodium Bicarbonate
NG	Natural Gas
Ni	Nickel
O_2	Oxygen
ODP	Ozone Depletion Potential
OER	Oxygen Evolution Reaction
OH^-	Hydroxide
PEEK	Poly Ether Ether Ketone
PEG	Polyethylene Glycol
PEM	Polymer Electrolyte Membrane
PEMEC	Proton Exchange Membrane Electrolyzer Cell
PET	Polyethylene Terephthalate
PFSA	Perfluorinated Sulfonic Acid
Pt	Platinum (nanoparticles)
Pt/C	Platinum-on-Carbon (or Platinum Black) catalyst
PTFE	Polytetrafluoroethylene
PTL	Porous Transport Layer
PVD	Physical Vapor Deposition
R&D	Research and Development
RuO_2	Ruthenium Dioxide
SMR	Steam Methane Reforming
SOE	Solid Oxide Electrolysis
SOEC	Solid Oxide Electrolysis Cell
TDS	Total Dissolved Solids
T_g	Transition Temperature
Y_2O_3	Yttrium Oxide (also called Yttria)
YSZ	Yttria-Stabilized Zirconia
Zirfon Perl UTP	ZrO_2 base, supported by polymer fabric in a mesh structure
ZrO_2	Zirconium Dioxide (also called Zirconia)

This page intentionally left blank.

ABSTRACT

The effects of climate change have led to a push for cleaner energy sources across multiple sectors. Hydrogen has emerged as a promising energy carrier in this context, as it can be produced using various water electrolysis technologies capable of utilizing clean power (e.g., nuclear and renewable electricity). However, a comprehensive environmental assessment of these technologies requires an understanding of the environmental impacts during their complete life cycle, including the embodied emissions in their material composition and during their manufacturing stages; these emissions are often neglected. This report provides a brief overview of major water electrolysis technologies, viz., proton exchange membrane electrolyzer cell (PEMEC) or polymer electrolyte membrane (PEM), alkaline electrolysis cell (AEC) and solid oxide electrolysis cell (SOEC), along with a detailed bill of materials for these technologies that has been incorporated in the updated Greenhouse gases, Regulated Emissions, and Energy use in Transportation (GREET®) 2022 model. We also provide an inventory for the intermediate materials used to produce these electrolyzers, which has not been covered in prior releases. Using these material and energy flows, the GREET model provides a detailed life cycle inventory (energy use and emissions) from raw material extraction through complete production of electrolyzers for major electrolysis technologies.

1 INTRODUCTION

The global focus on achieving net-zero carbon emission targets to avoid the worst effects of climate change has caused a major increase in the production and use of renewable energy technologies (Gerloff, 2021a; IPCC, 2021; Zhao et al., 2020). While the prime focus has been on wind and solar energy for electricity production, other alternative sources and carriers of energy have emerged in recent years. Of these, hydrogen (H_2) has emerged as a key carrier with significant potential for use across different sectors involving energy generation and consumption (Holst et al., 2021; Ruth et al., 2021). Given the intermittent nature of wind and solar energy, H_2 can be produced using these energy forms, stored in bulk quantities, and used to produce electricity for grid balancing, stability, and backup power needs (Gerloff, 2021b; Ruth et al., 2021; Zhao et al., 2020). H_2 produced using renewable energy can replace natural gas-based H_2 in current applications such as the production of plastics, chemicals, and fertilizers, and refining of oil and metals (Ruth et al., 2021). H_2 can also reduce carbon emissions from transportation by powering fuel-cell electric vehicles (FCEVs), and from natural gas via H_2 mixing within the pipeline supply for end users (Cetinkaya et al., 2012; Ruth et al., 2021).

The standard low-carbon technology used for H_2 production is water (H_2O) electrolysis, where electricity from renewables is used to split water into constituent H_2 and oxygen (O_2) gases (Gerloff, 2021b; Ruth et al., 2021). This type of H_2, termed *green hydrogen*, has been repeatedly highlighted to be beneficial to reducing greenhouse gas (GHG) emissions of H_2 production over the conventional steam methane reforming of natural gas (SMR-NG) (Bhandari et al., 2014; Cetinkaya et al., 2012; Ghandehariun and Kumar, 2016; Patyk et al., 2013; Peng and Wei, 2020). However, these studies focus primarily on the benefits accrued via the change in the energy source used for H_2 production. In contrast, only a handful of studies (Gerloff, 2021b; Patyk et al., 2013; Zhao et al., 2020) focus on GHG emissions during the production stages of water electrolysis technologies. This makes it difficult to (a) evaluate and compare the life cycle GHG emissions of H_2 production via water electrolysis technologies with that from SMR-NG, (b) determine the relative ranking of different water electrolysis technologies on their GHG footprint, and (c) assess the relative significance of production stages in life cycle GHG emissions of these technologies.

This report provides details for conducting a comprehensive life cycle analysis of GHG emissions of water electrolysis technologies that have been incorporated in Argonne's GREET® model update for the year 2022 (Wang et al., 2022). The rest of this report is organized as follows. Section 2 provides a description of currently commercial water electrolysis technologies, along with a brief literature review of assessments of their environmental impacts over different life cycle stages. In Section 3, we provide the material composition (bill of materials) for these water electrolysis technologies, based on our personal communication with Strategic Analysis, Inc. (Strategic Analysis, 2022). Finally, in Section 4, we provide the material and energy flows (or life cycle inventory, LCI) for the production of various intermediate materials that are used in H_2 production and that are currently unavailable in GREET model.

2 WATER ELECTROLYSIS TECHNOLOGIES

At present, three major electrolysis technologies are commercially available: (a) solid oxide electrolysis (SOE or SOEC, where C stands for cell), (b) proton exchange membrane electrolyzer cell (PEMEC) or polymer electrolyte membrane (PEM), and (c) alkaline electrolysis (AE or AEC) (Gerloff, 2021b; Ruth et al., 2021). These technologies differ in several ways, including process temperatures used, electrolytes employed, and their respective constituent materials. While PEMEC and AEC systems are considered low-temperature electrolysis systems, SOECs are referred to as high-temperature electrolysis systems. A succinct description of the general concepts behind these three technologies and their individual details is provided in the following sub-section. Subsequently, we discuss the current state of literature on the life cycle analysis of these technologies.

2.1 Description of Electrolysis Technologies

2.1.1 General Concept for All Technologies

Figure 1 shows the typical schematic of an electrolysis cell (Holst et al., 2021). This cell comprises four main components: (a) two metal electrodes—an oxygen electrode where oxygen evolution reaction (OER) occurs (anode), and a hydrogen electrode where hydrogen evolution reaction (HER) occurs (cathode), (b) an electrolyte that ensures ionic conductivity (or ion transfer), and (c) a thin material layer that is ion-conductive, called the separator (Grigoriev et al., 2020; Holst et al., 2021; Zhao et al., 2020). During electrolysis, a large direct current (DC) voltage is applied to the cell along with a simultaneous water supply. This causes redox reactions at the two electrodes, the net sum of which is the water decomposition reaction into H_2 and O_2 molecules at the cathode and anode respectively. While ions and electrons can permeate through the separator, gas permeation is substantially disabled, which significantly hinders the recombination of hydrogen and oxygen gases to form water (Grigoriev et al., 2020; Holst et al., 2021; Zhao et al., 2020).

Electrolysis cells can be of three types: (a) gap-cells, where there is a gap or distance between the electrodes and the separator, (b) zero-gap cell, where the electrodes are porous and pressed against the separator, and (c) PEMECs, where the membrane acts as both electrolyte and separator (Grigoriev et al., 2020). An assembly of numerous such cells is termed a *stack* (Grigoriev et al., 2020; Holst et al., 2021; Zhao et al., 2020). Other components—structural and auxiliary—are needed both at the stack level (i.e., assembly of numerous cells) and at the electrolyzer pack level (i.e., collection of multiple stacks) to ensure their desired functioning. These are described in the subsections below.

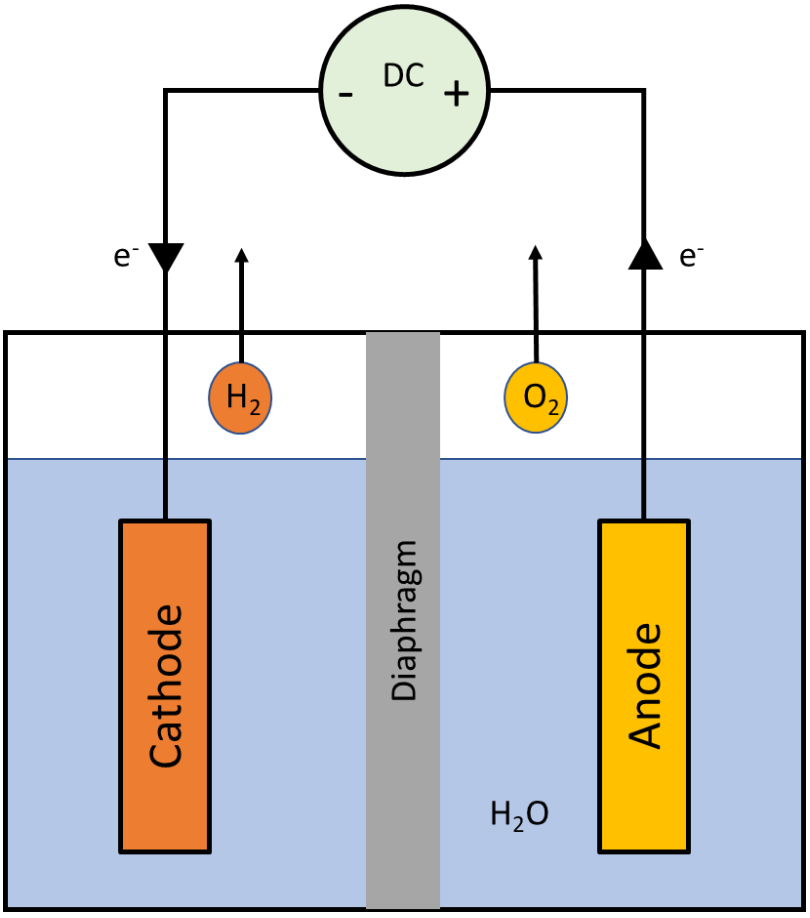

Figure 1: Basic structure of an electrolysis cell (developed based on image in (Holst et al., 2021)

2.1.2 Alkaline Electrolyzers (AE/AEC)

AEC is the oldest, most mature, and most widely deployed electrolyzer technology to date, having been in commercial use for over 100 years (Gerloff, 2021b; Grigoriev et al., 2020; Holst et al., 2021; Zhao et al., 2020). It is a low-temperature process (operating at 60°C-90°C) that employs an alkaline liquid electrolyte (20-40 wt.% potassium hydroxide or KOH) and operates at cell pressures from atmospheric pressure to 30 bar (Grigoriev et al., 2020; Holst et al., 2021). AEC has been mainly used for megawatt (MW)-scale H_2 production in industrial end uses, such as ammonia production (Holst et al., 2021). In AECs, water is typically supplied to the cathode, where it splits into H_2 gas and hydroxide (OH^-) ions (Holst et al., 2021). These OH^- ions pass through the diaphragm (anion conducting membrane) to get converted into O_2 and water at the anode.

Typically, AEC cells require the diaphragm (separator) and electrodes to be placed close to each other (sandwich-like structure), which is called *zero gap* design or diaphragm electrode assembly (DEA) (Holst et al., 2021; Zhao et al., 2020). This lowers both ionic resistance (via reduced distance between electrodes) and overpotential (via gas evolution at the back of the

electrodes), which together improves cell efficiency (Holst et al., 2021). Cell components are pressed together with spacers used between electrodes and cell housings (or bipolar plates) (Holst et al., 2021). While cells are mostly rectangular-shaped, round-shape cell designs can also be used at higher pressure levels to avoid leakage (Holst et al., 2021).

AEC electrodes are typically made from nickel or stainless steel due to a combination of high corrosion resistance, high electrical conductivity, and high electrochemical activity (Grigoriev et al., 2020; Holst et al., 2021; Zhao et al., 2020). This is complemented by use of electrocatalysts on base substrates to further enhance corrosion resistance and electrochemical activity (Holst et al., 2021). Typical catalysts for cathode include ruthenium dioxide (RuO_2), molybdenum (Mo), mixed metal oxides (MMOs), and nickel-alloys (such as Ni-Mo), while nickel- and/or nickel- and cobalt-oxide mixture is used as an anode catalyst (Gerloff, 2021b; Grigoriev et al., 2020; Holst et al., 2021; Zhao et al., 2020). Zirfon Perl UTP (ZrO_2 base supported by polymer fabric in a mesh structure) produced by the Agfa company is the most common diaphragm for AECs (Holst et al., 2021). This is mainly due to its high electrochemical, chemical, and thermal resistance, coupled with desired ion permeability. While bipolar plates and spacers are made from nickel and/or nickel-coated steel for high corrosion resistance against the electrolyte (KOH), gaskets are made from PTFE (polytetrafluoroethylene) or EPDM (ethylene propylene diene monomer) to prevent leakage (Gerloff, 2021b; Holst et al., 2021; Zhao et al., 2020).

At the stack level, AECs are connected in series (back side of cathode of one cell with anode of neighbor cell) by pressing concurrently such that individual cells are clamped between end plates and pressed with threaded rods that typically run over the entire stack length (Holst et al., 2021). Also, higher stack pressures are often preferred to enable more compact stack design.

2.1.3 Polymer Electrolyte Membrane or Proton Exchange Membrane (PEM/PEMEC) Electrolyzers

Unlike AECs, PEMECs are a relatively recent technology, first developed in the 1960s but gaining prominence in the 1970s through developments at General Electric (GE) using DuPont's Nafion® membrane (Grigoriev et al., 2020; Holst et al., 2021). While PEMECs are also a low-temperature technology (50°C -100°C) like AECs, they use a polymer electrolyte membrane instead of a liquid electrolyte like KOH (Bhandari et al., 2014; Gerloff, 2021b; Grigoriev et al., 2020; Holst et al., 2021; Zhao et al., 2020). Another point of difference with AECs is that here, water is supplied at the anodes for splitting into oxygen and hydrogen ions (H^+) (Grigoriev et al., 2020; Holst et al., 2021). While oxygen is discharged at the anode, H^+ ions move across the proton-conducting membrane (as the name implies) to the cathode and react with electrons to form hydrogen gas.

PEMEC electrodes are coated directly on the membrane, forming a membrane electrode assembly (MEA). The use of a solid electrolyte eliminates both the need for liquid electrolyte circulation and resistance caused by gas bubbles forming at the electrodes (Holst et al., 2021). Further, both the MEA arrangement and use of the solid electrolyte membrane together make the PEMEC and stack design more compact, while also ensuring adequate transfer of ions over a

wide range of current densities (Grigoriev et al., 2020; Holst et al., 2021). MEAs are compressed between porous transport layers (PTLs), which combine with an interconnect (bipolar plate) and a gasket to constitute a PEMEC stack (Holst et al., 2021; Zhao et al., 2020). The individual cells are connected both electrically (in series) and hydraulically (in parallel) to achieve high H_2 production rates (Holst et al., 2021). Also, higher pressures are used in PEMEC stacks (20-30 bars) than in their AEC counterparts (Grigoriev et al., 2020; Holst et al., 2021).

Typical membranes used in PEMECs are perfluorinated sulfonic acid (PFSA) membranes such as Nafion® (Bhandari et al., 2014; Grigoriev et al., 2020; Holst et al., 2021; Zhao et al., 2020). As these membranes are quite thin (100-200 µm thick), platinum nanoparticles (Pt) are used as recombination catalysts on the membrane to avoid any permeation of hydrogen through it (Grigoriev et al., 2020; Holst et al., 2021). Also, internal reinforcing structures are used in PFSA membranes to reduce any swelling in it due to water absorption (Holst et al., 2021). A platinum-on-carbon (or *platinum black*) catalyst (Pt/C) is used on the cathode for efficient H_2 production, while either iridium or ruthenium, and/or their oxides, is used as a catalyst for the anode (oxygen production), with iridium being the most preferred (Bhandari et al., 2014; Grigoriev et al., 2020; Holst et al., 2021). PTLs are also thin, like PFSA membranes (up to 100 µm thick), but are needed to ensure uniform current distribution between the electrodes and bipolar plate (Holst et al., 2021). For the cathode (hydrogen side electrode), carbon paper or non-woven carbon is used as a PTL, while titanium is the preferred PTL for the anode (oxygen side electrode) due to its high conductivity and corrosion resistance (Gerloff, 2021b; Grigoriev et al., 2020; Holst et al., 2021; Zhao et al., 2020). Titanium is also used to make bipolar plates for the same reason (Grigoriev et al., 2020; Holst et al., 2021).

2.1.4 Solid Oxide Electrolysis Cell (SOEC)

Unlike PEMECs and AECs, SOECs are high-temperature electrolyzer systems (operating at 600°C -1000°C) (Bhandari et al., 2014; Gerloff, 2021b; Grigoriev et al., 2020; Holst et al., 2021; Zhao et al., 2020). However, the SOEC is also the newest of the electrolyzer systems and is thus relatively immature compared to the other two technologies. Here, water is supplied to the cathode (as in PEMECs), where it receives electrons to produce hydrogen gas and oxygen anions (Grigoriev et al., 2020; Holst et al., 2021). These oxygen anions move to the anode, where they lose their excess electrons to be emitted as oxygen gas.

The high-temperature operation of SOECs is beneficial for H_2 production over the two low-temperature technologies (PEMEC and AEC) in multiple ways. First, the use of a high temperature reduces the equilibrium cell voltage needed to split water by providing the residual energy needed as heat (Grigoriev et al., 2020). Higher temperatures also significantly address the kinetic limitations associated with the transfer of ions, electrons, and gases and the resultant electrochemical reaction in cells (Grigoriev et al., 2020). Further, water splitting reactions in SOECs occur in the vapor phase (instead of the liquid phase in PEMEC and AEC), where the free energy needed for this reaction is lower (Grigoriev et al., 2020). Also, a considerable chunk of this energy can be provided using heat (thermally) instead of electricity (Grigoriev et al., 2020), which lowers electricity-related costs and effects. Finally, unlike PEMEC and AEC technologies, SOEC stacks generate high-temperature heat, which is suitable for integration with

heating systems for offices associated with the electrolyzer plant, thus optimizing the energy consumption of overall setup (Gerloff, 2021b; Grigoriev et al., 2020; Zhao et al., 2020).

Typical SOEC electrolytes consist of doped zirconia (ZrO_2), with the main dopant being yttria (Y_2O_3) (Bhandari et al., 2014; Gerloff, 2021b; Zhao et al., 2020). The cathode (hydrogen electrode) usually contains both zirconia and nickel (Ni), while the anode (oxygen electrode) material is generally lanthanum-based perovskites, such as lanthanum strontium cobalt ferrite (LSCF) or lanthanum strontium chromite (LSC) (Bhandari et al., 2014; Gerloff, 2021b; Grigoriev et al., 2020; Zhao et al., 2020). Ceria (CeO_2) is also added as a catalyst, often in doped form (e.g., gadolinium-doped ceria), to (a) raise the ionic conductivity of the cell and (b) form an inter-layer between the anode and electrolyte to prevent the formation of any electrically resistive zirconates (Zhao et al., 2020).

At the level of stacks, interconnects made from ferritic stainless steels (with high chromium or Cr content) are used (Zhao et al., 2020). These usually have a cobalt-rich coating (that contains cerium/Ce and/or manganese/Mn) to both prevent corrosion and protect the anode (oxygen electrode) from Cr, as it can block the reaction sites for oxygen evolution. Glass ceramics are used to hold the cells, frames, and interconnects in place over the entire stack lifetime (Zhao et al., 2020).

Cells are themselves made using ceramic powders that are shaped into layers using a variety of processes (such as tape casting and spraying) and organic materials (such as solvents and binders) (Zhao et al., 2020). These cells are adhered to a steel frame and assembled with other components (e.g., spacers). Upon stacking, the stack is mechanically compressed and then heated to its glass transition temperature (T_g) to ensure sufficient gas tightening between components adjacent to each other (Zhao et al., 2020).

Table 1 shows the specific features of all electrolyzer technologies, along with their respective advantages and limitations, based on various references (Gerloff, 2021b; Grigoriev et al., 2020; Holst et al., 2021; IEA, 2019).

2.1.5 Balance of Plant (BOP) Components

No electrolyzer stack is used by itself, as they need a number of auxiliary systems that can enable continuous hydrogen production. These systems are called balance of plant (BOP) components and can differ across the three aforementioned electrolyzer technologies (Gerloff, 2021b; Holst et al., 2021). Nevertheless, most of the BOP components are common across these technologies (though the actual number of these systems can vary based on both technology and size of stack or quantity of H_2 produced) (Holst et al., 2021). Table 2 provides a list of these components as well as their major functions (Holst et al., 2021).

Table 1: Key features of different water electrolyzer technologies (based on (Gerloff, 2021b; Grigoriev et al., 2020; Holst et al., 2021; IEA, 2019))

Parameters	Types of water electrolyzer technologies		
	Alkaline (AEC)	**Proton exchange membrane or Polymer electrolyte membrane (PEMEC)**	**Solid oxide electrolyzer cell (SOEC)**
Technology status	Mature, state-of-the-art	Demonstration/ commercially available	Lab-scale and in research and development (R&D)
Overall reaction	$H_2O \rightarrow H_2 + 1/2\,O_2$		
Reaction at anode	$2OH^- \rightarrow 1/2\,O_2 + H_2O + 2e^-$	$H_2O \rightarrow 1/2\,O_2 + 2e^- + 2H^+$	$O^{2-} - 2e^- \rightarrow 1/2\,O_2$
Reaction at cathode	$2H_2O + 2e^- \rightarrow H_2 + 2OH^-$	$2H^+ + 2e^- \rightarrow H_2$	$H_2O + 2e^- \rightarrow H_2 + O^{2-}$
Charge carrier	OH^-	H^+	O^{2-}
Cathode catalyst	Ni foam Ni-stainless steel Ni-Mo ZrO_2-TiO_2	Platinum	Ni-YSZ Ni-GDC cermet (gadolinia-doped ceria)
Anode catalyst	Ni_2CoO_4, La-Sr-CoO_3, Co_3O_4	Iridium oxide Ruthenium oxide	(La, Sr) MnO_3, (La, Sr)(Co,Fe)O_3
Electrolyte used	20-40 wt.% KOH (aqueous)	Perfluorinated sulfonic acid (PFSA)	Yttria-stabilized zirconia (YSZ) Sc_2O_3-ZrO_2 MgO-ZrO_2 CaO-ZrO_2
Separator material	ZrO_2 on polyphenylsulfone Asbestos Polysulfone-bonded poly-antimonic acid NiO Polysulfone impregnated with Sb_2O_5 polyoxide	Polymer membrane	Ceramic
Sealant	Metallic	Synthetic rubber Fluoroelastomer	Glass Vitro-ceramics
Current distributor	Ni	Titanium	Ferritic stainless steel
Containment material	Ni plated steel	Stainless steel	Stainless steel

Table 1 (Cont.)

Parameters	Types of water electrolyzer technologies		
	Alkaline (AEC)	**Proton exchange membrane or Polymer electrolyte membrane (PEMEC)**	**Solid oxide electrolyzer cell (SOEC)**
Operational temperature range (°C)	60-90	50-100	650-1000
Range of pressure (bar)	1-30	30-80	1
Current density (conventional, A/cm^2)	0.2-0.6	0.0-3.0 (up to 20)	0.0-2.0
Efficiency (%) (at $iA/cm^2/U_{cell}$ V/T °C)	60-80 0.2-0.5/2.0/80	80 1.0/1.8/65	> 99% 3.6/1.48/950
Capacity (Nm^3/h)	1-500	1-250	1
Lifetime (h)	60,000-90,000	30,000-90,000	10,000-30,000
H_2O form (specification)	Liquid	Greater than 10 MΩ cm	Steam
Load cycling	Medium	Good	Good
Stop/go cycling	Weak	Good	Weak
Temperature cycling	Weak	Good	Weak
Cell voltage (V)	1.8-2.4	1.8-2.2	0.95-1.3
Power density (W/cm^2)	Up to 1.0	Up to 4.4	
Voltage efficiency (%)	62-82	67-82	81-86
Specific energy consumption (system, kWh/Nm^3)	4.5-7.0	4.5-7.5	2.5-3.5
Partial load range (%)	20-40	0-10	
Cell area (m^2)	< 4	< 300	
Hydrogen production rate (Nm^3/h)	< 760	< 30	
System lifetime (year)	20-30	10-20	
Purity of H_2 produced (%)	More than 99.8%	99.999	
Cold start up time (min)	15	< 15	> 60
Plant footprint (m^2/kW_e)	0.095	0.048	
Capital expenditure (CAPEX) ($/$kW_e$)	500-1,400	1,100-1,800	2,800-5,600

Table 2: Balance of plant (BOP) components (Holst et al. (2021))

Bop components	Description/Key Features
Transformer/power electronics	• Converts the alternating current (AC) supply from the electric grid to the direct current (DC) supply needed for commercial electrolysis by using thyristor-based rectifiers. • Rectifier voltage capacity must range between minimum stack voltage (start-of-life and partial load) and maximum stack voltage (end-of-life) for uninterrupted AC-to-DC conversion over stack lifetime. • Filter circuits used in tandem with rectifiers to lower reactive effects of converters.
Water purification system	• Purifies water by removing all contaminants in the supplied water that can deactivate catalysts and thereby significantly degrade the electrolysis cells. • Typically applied to tap water supply that is highly stable, inexpensive, and involves fewer regulations • Recommended values: conductivity – 0.1-1 µS/cm and total dissolved solids (TDS) < 0.5 ppm. • Additional systems needed for specific electrolyzer technologies (e.g., ion-exchanger for PEMs) to maintain the desired water quality for electrolysis.
Hydrogen purification system	• Purifies hydrogen to high levels by removing both the oxygen (transferred from anode to cathode in electrolysis stack) and water content from it. • Involves two steps: (a) removal of oxygen using a deoxygenation reactor (where oxygen is trapped on a palladium catalyst used on alumina) and (b) water adsorption (using materials like silica gel).
Cooling system	• Cools stacks (which constantly generate heat), product gases (to condense water and send it back to the electrolyzer), H_2 purification unit, and compression system. Dissipated heat is usually used for space heating. • Typically conducted using dry coolers that chill the coolant (water or ethylene glycol) to near-ambient temperature, though industrial cooling machines are also used to cool product gases.
Compression system	• Pressurizes gas to 80-900 bars for optimal storage of H_2 in tanks for subsequent transport and processing • Involves multi-stage, reciprocal compressors powered by electrical motors.

2.2 Literature Review: Life-Cycle Analysis of Electrolyzer Technologies

Multiple studies have investigated the life cycle environmental impacts of different electrolysis technologies. However, most of these studies have focused on the effect of the energy source used for electrolysis (Bhandari et al., 2014; Frank et al., 2021; Ghandehariun and Kumar, 2016; Mehmeti et al., 2018). In contrast, only a few studies have analyzed the inventory and resultant impacts of producing these electrolyzer technologies (stacks and BOP). Here, we focus on these studies and their respective findings.

Patyk et al. (2013) conducted life cycle analysis (LCA) of H_2 generation using high-temperature electrolysis technologies. Their study assumes a number of scenarios for the energy source used to provide electricity for electrolysis, including nuclear energy, wind power and water, wind power + water + biogas, and SMR (Patyk et al., 2013). They highlight stack manufacturing as the biggest contributor to GHG impacts during the production of SOEC plant (stack + BOP), and H_2 production (i.e., the nature of the electricity used) as the biggest influencer on life cycle impacts of SOECs (Patyk et al., 2013). Among energy sources, only wind-powered SOECs show lower energy use than SMR (Patyk et al., 2013). The reverse is seen for GHG impacts, with SMR showing the highest impact and nuclear power-based electrolysis showing the lowest.

Zhao et al. (2020) conducted LCA of all the three electrolyzer technologies (SOEC, PEMEC, and AEC) on 16 impact categories. They provide a detailed inventory (or bill of materials) for each of these technologies. The global warming potential (GWP) results for all stages, beginning with material extraction and ending with electrolyzer manufacturing, highlight strong contributions from: (a) stainless steel in interconnects and frame components on SOEC impacts, (b) oxygen electrodes (made from iridium, titanium, and platinum), interconnects (titanium with Pt coating), and hydrogen electrodes (Pt catalyst) on PEMEC impacts, and (c) Ni-containing components (interconnect, electrodes, and frame) on AEC impacts (Zhao et al., 2020). The same materials/components are also reported to play a significant role in other environmental impact categories, complemented by contributions from the nickel catalyst to SOEC impacts (Zhao et al., 2020). Their analysis also shows PEMECs to exhibit the highest GHG impacts among all three electrolyzer technologies (Zhao et al., 2020). In terms of life cycle impacts (including hydrogen production via electrolysis), electricity consumed for H_2 production accounts for the largest GHG and most other impacts across all electrolyzer technologies (Zhao et al., 2020).

Bareiß et al. (2019) have investigated the life cycle environmental impacts of H_2 production using PEMEC technology and compared it with impacts from SMR. They provide a detailed material composition of PEMECs with 1 MW capacity for the stack and BOP, and conducted LCA for three scenarios (2017 baseload, 2050 baseload, and 2050–3,000 h of operation) (Bareiß et al., 2019). Their study highlights a negligible effect of combined stack and BOP components on life cycle GHG emissions from this technology, independent of the scenario considered, with electricity used for electrolysis dominating these impacts (Bareiß et al., 2019). They also report the same observation for most other impacts in their study. However, in some categories, they observe a major difference in the form of electrolyzer systems accounting for a

significant chunk of life cycle impacts, such as BOP accounting for vast majority of ozone depletion potential (ODP) impacts in 2050 – 3,000 h scenario) (Bareiß et al., 2019).

Gerloff (2021b) conducted LCAs of PEMEC, AEC, and SOEC technologies, including both stack and BOP components/systems, over different energy scenarios for Germany. The study provides a detailed inventory for most stack and BOP components (Gerloff, 2021b). It also highlights a consistent decline in GHG emissions with an increasing use of renewables in the electric grid and reports that PEMECs exhibit the highest life cycle GHG emissions among all three electrolyzers (Gerloff, 2021b). The study also covers other kinds of impacts such as ODP and ionizing radiation (IR) (Gerloff, 2021b). However, it does not provide details on GHG impacts from the production of electrolyzers or the major contributors to these production-related impacts, although it does report components that play a significant role on any impact category (e.g., tetrafluoroethylene production on ODP) (Gerloff, 2021b). Overall, the study ranks AECs as the most environmentally unfriendly technology, with SOEC and PEMECs having a shift in their comparative environmental credentials with changes in their grid mix (Gerloff, 2021b).

3 BILLS OF MATERIALS FOR DIFFERENT ELECTROLYZER TECHNOLOGIES

We obtained detailed bills of materials (BOMs) for the stacks of all three electrolyzer technologies from SA, along with their respective stack input power capacities (in kW) and electricity consumed for stack manufacturing (in kWh) (Strategic Analysis, 2022). SA obtained this data from their internal model for various electrolyzers. Tables 3-5 provide the BOMs for AEC, PEMEC, and SOEC stacks as obtained from SA, segregated by component (Strategic Analysis, 2022). Two BOMs are provided for each stack—one for the exact stack weight and one that includes the weight of the waste generated in the production of the stack (i.e., stack weight + waste weight). Table 6 provides the stack power capacities (or system power capacity) and electricity consumption for stack manufacturing for all electrolyzers, assuming an annual electrolyzer production capacity of 700 MW/year (Peterson et al., 2020b, 2020a; Vickers et al., 2020).

In contrast to stacks, SA does not have any data on the weight and material composition of BOP components, or the energy needed to manufacture these BOP components, for any of the electrolyzer technologies. Hence, we used the detailed data for BOP components provided in Gerloff (2021b) in a three-step methodology to determine the weight, material composition, and manufacturing-related energy consumption for BOP of all electrolyzers. The variables used for this methodology are provided in Table 7.

$$\frac{X_{Scaled}}{X_{Gerloff}} = \left(\frac{C_{SA}}{C_{Gerloff}}\right)^{b} \quad (1)$$

First, we obtained the total weight and material composition of both stacks and BOP components for all electrolyzer technologies (with each technology having 1 MW system capacity) from Gerloff (2021b) (i.e., $SW_{Gerloff}$, and $SEC_{Gerloff}$). Gerloff (2021b) also provides data on the amount of energy (electricity) consumed to manufacture the stack and BOP (on a per-kW system capacity basis) for all technologies (i.e., $BOP - W_{Gerloff}$, and $BOP - EC_{Gerloff}$). Table 8 provides these weights and manufacturing-related energy consumption values for stacks and BOP of all electrolyzers from Gerloff (2021b). Next, we used Equation 1 from Gerloff (2021b) to scale the weight and manufacturing energy consumption for the stack and BOP of all electrolyzers (in Table 8) to system capacity values provided by SA (Table 6) (Strategic Analysis, 2022). Here, in Equation 1, we used the system (stack) input power capacities provided by SA (C_{SA}) and Gerloff (2021b) ($C_{Gerloff}$), along with scaling factor (b) values from Gerloff (2021b) for BOP and stack, with X_{Scaled} being SW_{Scaled}, SEC_{Scaled}, $BOP - W_{Scaled}$, or $BOP - EC_{Scaled}$, and $X_{Gerloff}$ correspondingly being $SW_{Gerloff}$, $SEC_{Gerloff}$, $BOP - W_{Gerloff}$, or $BOP - EC_{Gerloff}$. The scaled weights and manufacturing energy use (W_{Scaled}, SEC_{Scaled}, $BOP - W_{Scaled}$ and $BOP - EC_{Scaled}$) were used to obtain ratios of (a) BOP weight-to-stack weight ($W_{BOP-to-Stack}$) and (b) energy consumption for stack manufacturing-to-energy consumption for BOP production ($EC_{Stack-to-BOP}$). These ratios are given in Table 9.

Table 3: BOM or material composition of AEC stacks per SA (Strategic Analysis, 2022)

Component or Process Aspect	Material	Process Used	Per-Stack Weight (lb)	
			Excludes Waste Weight	Includes Waste Weight
Anode + cathode perforated plate	Ni	Stamping	1,935.44	1,935.44
Diaphragm	Agfa Zirfon Perl UTP 500	Purchased	305.96	305.96
Anode catalyst	$Ni(NO_3)_2$		3.45	3.52
	$Co(NO_3)_2$		5.74	5.85
	$Ru(NO_3)_2$		1.90	1.95
	Water		0.00	0.32
Cathode catalyst	NiAlMo	Atmospheric plasma spray coating	166.34	498.66
Elastic element	Ni	Purchased	18,816.67	18,816.67
Bipolar plate	Ni	Etching	5,692.89	7,869.40
Photoresist	Polypropylene	Etching	0.00	1,113.82
Etching solution	3% Sulfuric Acid	Etching	0.00	506.09
Subgasket	EPDM	Die cutting	1,971.62	4,913.66
Cell frame	Poly ether ether ketone (PEEK)	Injection molding	2,653.55	2,758.49
Gasket seal	EPDM	Die cutting	1,577.30	3,930.93
End gasket	EPDM	Die cutting	5.78	14.33
End plate	Stainless Steel 316	Machining	1,995.05	2,951.50
Dummy cell gasket	EPDM	Die cutting	11.55	28.66
Current collector	Copper	Current collector preparation	158.18	181.93
Insulator	PEEK	Injection molding	7.87	8.16
Stack insulation housing	Polypropylene	Injection molding	198.55	199.65
Locknut	Stainless Steel	Stack assembly	146.70	146.70
Belleville washer	Stainless Steel	Stack assembly	107.39	107.39
Tie rod + heat shrink	Stainless Steel		2,511.13	2,511.13
	PTFE		10.27	10.27
Total stack weight			**38,283.32**	**48,820.48**

Table 4: BOM or material composition of PEMEC stacks per SA (Strategic Analysis, 2022)

Component or Process Aspect	Material	Process Used	Per-Stack Weight (lb)	
			Excludes Waste Weight	Includes Waste Weight
Cathode PTL gas diffusion layer (GDL)	SGL carbon: GDL 34 BA (non-woven)	GDL preparation	4.80	8.00
	PTFE		1.04	1.25
	Methanol (solvent)		0.00	5.26
	Deionized (DI) water (solvent)		0.00	5.26
	Vulcan XC-72		0.80	0.97
Anode PTL + coating	Titanium powder	Dispensing & compacting Ti powder physical vapor deposition (PVD)	125.05	125.05
	Adhesive powder (polyurethane)		0.57	0.57
	Lubricant powder (zinc stearate)		0.64	0.64
	Pt coating		0.25	0.41
Membrane	ePTFE	Membrane preparation	1.25	1.96
	Nafion		21.78	35.49
	DI water (solvent)		0.00	3.19
	Hexanol (solvent)		0.00	0.11
	Isopropanol (solvent)		0.00	335.50
	Methanol (solvent)		0.00	335.43
Anode + cathode catalyst	Iridium powder (anode)	Slot die coating	1.21	6.00
	Methanol (solvent)		0.00	31.11
	DI water (solvent)		0.00	31.11
	Nafion		5.51	7.76
	CeO_2 additive		0.05	0.07
	Pt/C powder (cathode)		0.66	4.70

Table 4 (Cont.)

Component or Process Aspect	Material	Process Used	Per-Stack Weight (lb)	
			Excludes Waste Weight	Includes Waste Weight
Bipolar plate	Titanium grade 2	Etching	237.81	359.46
Photoresist	Polypropylene	Etching	0.00	100.48
Etching solution	3% sulfuric acid	Etching	0.00	561.23
Bipolar plate coating	Au coating (cathode)	PVD	0.03	0.05
	Pt coating (anode)		0.03	0.05
Sub-gasket + coolant gasket	Polyethylene terephthalate (PET)	Cutting/robot screen printing	9.90	25.86
	Polyolefin elastomer		2.82	5.86
O_2 cell frame	High-density polyethylene (HDPE)	Injection molding	30.18	37.50
H_2 cell frame	HDPE	Die cutting	2.12	8.35
Gasket seal	PET	Die cutting	34.87	137.41
End gasket	Polyolefin elastomer	Screen printing	0.01	0.02
End plate	Stainless steel 316	Machining	126.53	189.48
Dummy cell gasket	HDPE	Insertion molding	0.11	0.14
Current collector	Copper	Current collector preparation	11.86	13.62
Insulator	HDPE	Injection molding	0.50	0.57
Stack insulation housing	Polypropylene	Injection molding	17.74	18.06
Locknut	Stainless steel	Stack assembly	0.37	0.37
Belleville washer	Stainless steel	Stack assembly	1.51	1.51
Tie rod + heat shrink	Stainless steel	Stack assembly	30.25	30.25
	PTFE		0.62	0.62
Total Stack Weight			**670.87**	**2,430.68**

Table 5: BOM or material composition of SOEC stacks per SA (Strategic Analysis, 2022)

Component or Process Aspect	Material	Process Used	Per-Stack Weight (lb)	
			Excludes Waste Weight	Excludes Waste Weight
Electrolyte layer slurry	8-YSZ (56%)	Electrolyte layer slurry ball mill	0.41	0.41
	Xylenes solvent (17%)		0.00	0.13
	Ethanol solvent (16%)		0.00	0.12
	Phthalate plasticizer (4%)		0.00	0.03
	Glycol plasticizer (3%)		0.00	0.02
	Aldehyde binder (2%)		0.00	0.01
	PS-236 surfactant (2%)		0.00	0.01
Hydrogen electrode support layer slurry	NiO (37%)	Hydrogen electrode support layer slurry ball mill	11.60	11.60
	3-YSZ (28%)		8.78	8.78
	Methyl ethyl ketone solvent (17%)		0.00	5.33
	Ethanol solvent (8%)		0.00	2.51
	Aldehyde binder (3%)		0.00	0.94
	Polyethylene glycol (PEG) surfactant (3%)		0.00	0.94
	Phthalate plasticizer (2%)		0.00	0.63
	Glycol plasticizer (2%)		0.00	0.63
Hydrogen electrode functional layer slurry	NiO (37%)	Hydrogen electrode functional layer slurry ball mill	0.81	0.81
	8-YSZ (28%)		0.62	0.62
	Methyl ethyl ketone solvent (17%)		0.00	0.37
	Ethanol solvent (8%)		0.00	0.18
	Aldehyde binder (3%)		0.00	0.07
	PEG surfactant (3%)		0.00	0.07
	Phthalate plasticizer (2%)		0.00	0.04
	Glycol plasticizer (2%)		0.00	0.04

Table 5 (Cont.)

Component or Process Aspect	Material	Process Used	Per-Stack Weight (lb)	
			Excludes Waste Weight	Excludes Waste Weight
Hydrogen electrode contact layer slurry	NiO (60%)	Hydrogen electrode contact layer slurry ball mill	3.51	3.51
	Terpineol solvent (40%)		0.00	2.34
Barrier layer slurry	Gadolinium-doped ceria (GDC): GDC (61%) ethanol solvent (19%) methyl ethyl ketone solvent (9%) aldehyde binder (5%) phthalate plasticizer (2%) glycol plasticizer (2%) PS-236 surfactant (2%)	Barrier layer slurry ball mill	0.38	0.62
Air electrode layer slurry	LSCF-GDC: LSCF (46%) GDC (20%) Ferro BD75-717 ink vehicle (34%)	Air electrode layer slurry ball mill	1.71	2.59
Air electrode contact layer slurry	GDC: GDC (60%) Terpineol solvent (40%)	Air electrode contact layer slurry ball mill	1.89	3.15
Tape casting film	Mylar	Tape casting	0.00	5.45
Interconnect	Hitachi ZMG-G10	Etching	60.10	78.00
Photoresist	Polypropylene	Etching	0.00	26.12
Etching solution	$NaNO_3$/NaCl mixture	Etching	0.00	1.04

Table 5 (Cont.)

Component or Process Aspect	Material	Process Used	Per-Stack Weight (lb)	
			Excludes Waste Weight	Excludes Waste Weight
MCO interconnect coating	MCO: $CoCO_3$ (11%) $MnCO_3$ (10%) Glycine (44%) Nitric acid (35%)	Combustion + PVD	0.43	3.47
Glass seal slurry	SCHOTT G018-311: SCHOTT G018-311 glass powder (72%) Heraeus V-006A lower viscosity vehicle (28%)	Glass seal slurry ball mill	0.90	1.24
End plate	Alloy 600	End plate machining	28.53	34.25
Corrosion resistant tension rod	Stainless steel	Stack assembly	9.52	10.03
Pressure spring	Stainless steel	Stack assembly	0.07	0.07
Small parts	Stainless steel sleeve bearing (40%)	Stack assembly	0.88	0.88
	Stainless steel nut (30%)		0.66	0.66
	Alumina ceramic spacer (20%)		0.44	0.44
	Stainless steel washer (10%)		0.22	0.22
Ceramic fiber insulation sheet	UniTherm aluminum silicate fiber	Stack assembly	1.68	1.90
Piping	Stainless steel 430	Stack assembly	1.42	1.42
Gas	2% H_2 in N_2	Stack braze	0.00	1.41
Total Stack Weight			**134.56**	**213.11**

Table 6: Stack capacity and electricity manufacturing per SA (Strategic Analysis, 2022)

Parameters	AEC	PEMEC	SOEC
System (stack) input power (kW)	3,836	998	50
Stack manufacturing energy consumption (kWh)	77,326	5,302	770

Table 7: Variables used in calculation of BOP weight

Variables	Description
SW_{SA}	Stack weight for any electrolyzer per SA
SEC_{SA}	Energy consumed to manufacture and assemble stack for any electrolyzer per SA
$BOP - W_{SA}$	Weight of BOP for any electrolyzer per SA
$BOP - EC_{SA}$	Energy consumed to manufacture BOP components and assembly per SA
$SW_{Gerloff}$	Stack weight for any electrolyzer, per Gerloff (2021b)
$SEC_{Gerloff}$	Energy consumed to manufacture and assemble stack per kW of system capacity for any electrolyzer, per (Gerloff, 2021b)
$BOP - W_{Gerloff}$	Weight of BOP for any electrolyzer, per Gerloff (2021b)
$BOP - EC_{Gerloff}$	Energy consumed to manufacture BOP components and assembly per kW of system capacity for any electrolyzer, per Gerloff (2021b)
SW_{Scaled}	Stack weight for any electrolyzer, obtained using Equation 1
SEC_{Scaled}	Energy consumed to manufacture and assemble stack for any electrolyzer, obtained using Equation 1
$BOP - W_{Scaled}$	Weight of BOP for any electrolyzer, obtained using Equation 1
$BOP - EC_{Scaled}$	Energy consumed to manufacture BOP components and assembly, obtained using Equation 1
C_{SA}	System input power capacity, as provided by SA
$C_{Gerloff}$	System input power capacity, as provided by Gerloff (2021b)
$W_{BOP-to-Stack}$	Ratio of weight of BOP to weight of stack (for any electrolyzer)
$EC_{Stack-to-BOP}$	Ratio of manufacturing-related energy consumption for stack to that for BOP (for any electrolyzer)

Table 8: Weight and manufacturing-related energy consumption of electrolyzer stack and BOP per (Gerloff, 2021b)

Parameter	Variable	Electrolyzer Technologies		
		AEC	PEMEC	SOEC
Stack weight (lb)	$SW_{Gerloff}$	51,468	1,522	20,844
BOP weight (lb)	$BOP - W_{Gerloff}$	87,384	42,351	102,255
System capacity (kW)	$C_{Gerloff}$	1,000	1,000	1,000
Energy consumed for stack manufacturing (mmBtu/kW)	$SEC_{Gerloff}$	0.75	0.81	0.95
Energy consumed for BOP manufacturing (mmBtu/kW)	$BOP - EC_{Gerloff}$	0.13	0.17	0.26

Table 9: Scaling factor and electrolyzer stack and BOP parameters used in the updated GREET model (based on SA data)

Parameter	Variables	Electrolyzer technologies		
		AEC	PEMEC	SOEC
Scaling factor—BOP (Gerloff, 2021b)	b	0.7	0.7	0.7
Scaling factor—stack (Gerloff, 2021b)	b	0.88	0.88	0.88
Stack weight per SA (lb/stack)	SW_{SA}	38,283.3	670.9	134.6
Energy consumed for stack manufacturing per SA (mmBtu/stack)	SEC_{SA}	263.6	18.1	2.6
Ratio: BOP weight-to-stack weight	$W_{BOP-to-Stack}$	1.3	27.8	8.4
Ratio: Manufacturing energy consumption—stack to BOP	$EC_{Stack-to-BOP}$	26.1	16.5	7.4
BOP weight (lb/stack)	$BOP - W_{SA}$	51,028.1	18,679.2	1,131.9
Energy consumed for BOP production (mmBtu/stack)	$BOP - EC_{SA}$	10.1	1.1	0.4

In the final step, we used these ratios on stack weight (SW_{SA}) and stack manufacturing energy consumption (SEC_{SA}) given by SA (Strategic Analysis, 2022) to compute the weight ($BOP - W_{SA}$) and manufacturing energy usage ($BOP - EC_{SA}$) for BOP systems of all electrolyzer technologies (also given in Table 9). This was done to size the BOP system in line with the stack system given by SA. The material composition of all BOP systems is assumed to be the same as that of the BOP in (Gerloff, 2021b), regardless of the actual change in its total weight. Tables 10–12 provide the material composition of BOP systems for all three electrolyzer technologies. It is the weight, material composition, and energy consumption values provided in Tables 9–12 that are used in the updated GREET model for 2022. Please note that the weights of different materials are provided on a per-pound basis for both stack and BOP. Note that since the BOM for the BOP is based on an external reference instead of SA's data, its material inputs and resultant energy use and emission impacts have been greyed out in the GREET 2022 release. Efforts will be made to secure the BOMs for BOP components of all three electrolyzer systems from SA and update these in future GREET versions.

Table 10: Material composition of BOP system for AEC electrolyzer (based on (Gerloff, 2021b))

Materials	Wt.% share in BOP
Concrete	46.7
Steel	31.5
Stainless steel	16.9
Copper	1.6
Extruded HDPE	1.2
Glass fiber	1.2
Elastomer	0.5
Wrought Al	0.4
Ethylene glycol	0.02
Injection molded PP	0.01

Table 11: Material composition of BOP system for PEMEC electrolyzer (based on (Gerloff, 2021b))

Materials	Wt.% share in BOP
Steel	39.0
Concrete	29.2
Stainless steel	22.5
Extruded HDPE	2.4
Copper	1.8
Injection molded PP	1.6
Wrought aluminum	1.4
Elastomer	0.6
Lubricating oil	0.5
Zeolite	0.5
Electronics	0.5
Ethylene glycol	0.003

Table 12: Material composition of BOP system for SOEC electrolyzer (based on (Gerloff, 2021b))

Materials	Wt.% share in BOP
Stainless steel	35.8
Steel	22.4
Cold-rolled steel	21.2
Concrete	12.1
Hot-rolled steel	4.9
Extruded LDPE	1.2
Copper	0.9
Aluminum (sheet/wrought)	0.8
Elastomer	0.4
Controller	0.2
Ethylene glycol	0.1
Acrylonitrile-butadiene (injection molding)	0.003

4 INTERMEDIATE MATERIALS

4.1 Sodium Bicarbonate

Sodium bicarbonate ($NaHCO_3$) is typically produced by reacting sodium carbonate (or soda ash) (Na_2CO_3) with water (H_2O) and carbon dioxide (CO_2) (Biganzoli et al., 2015), with the reaction shown below. Table 13 shows the material and energy flows for production of sodium bicarbonate (Biganzoli et al., 2015).

$$Na_2CO_3 + H_2O + CO_2 \rightarrow 2NaHCO_3$$

4.2 Cobalt Carbonate

Cobalt carbonate ($CoCO_3$) is industrially produced by reacting cobalt sulfate ($CoSO_4$) and sodium bicarbonate ($NaHCO_3$), as shown below (Donaldson and Beyersmann, 2005). The reaction also yields sodium sulfate (Na_2SO_4), water (H_2O), and carbon dioxide (CO_2) as shown below. Table 13 shows the material flows associated with cobalt carbonate production, based on chemical reaction stoichiometry. No energy flows are given due to a lack of data in the literature.

$$CoSO_4 + 2NaHCO_3 \rightarrow CoCO_3 + Na_2SO_4 + H_2O + CO_2$$

4.3 Dichloromethane

Dichloromethane (CH_2Cl_2) is used as an input for terpineol production (Alberola-Borràs et al., 2018; Parvatker and Eckelman, 2020), which is itself an intermediate solvent used in electrolyzer production (Strategic Analysis, 2022). Dichloromethane is usually produced via reaction between methane (CH_4) and chlorine (Cl_2), with the reaction also yielding hydrochloric acid (HCl) (Parvatker and Eckelman, 2020), as shown below. Table 13 provides the material flows for dichloromethane production based on reaction stoichiometry, with no energy flows provided due to a paucity of data.

$$CH_4 + 2Cl_2 \rightarrow CH_2Cl_2 + 2HCl$$

4.4 Terpineol

Terpineol is a solvent that is produced using dichloromethane, acetone, acetylene, liquid hydrogen, and water (Alberola-Borràs et al., 2018). Table 13 provides the material and energy flows for production of terpineol (Alberola-Borràs et al., 2018).

4.5 Manganese Carbonate

Manganese carbonate ($MnCO_3$) is produced through reaction between manganese sulfate ($MnSO_4$) and alkali-metal carbonates (such as sodium carbonate) and/or alkali-metal hydrogen carbonates, such as sodium bicarbonate ($NaHCO_3$) (Norkem, 2022). The reaction also yields sodium sulfate (Na_2SO_4), water (H_2O), and carbon dioxide (CO_2), as shown in the equation below. Table 13 shows the material flows for manganese carbonate production based on reaction stoichiometry; no energy flows are shown due to lack of data.

$$MnSO_4 + 2NaHCO_3 \rightarrow MnCO_3 + Na_2SO_4 + H_2O + CO_2$$

4.6 Yttria-Stabilized Zirconia (YSZ)

Two forms of YSZ—8 mol.% and 3 mol.%—are used in SOEC electrolyzers. Since the inventory for both yttria and zirconia are present in the GREET model, these are used in the respective mass ratios to obtain the final inventory for these materials (hence, their material and energy flow is not separately included in this report).

4.7 Isopropanol

Isopropanol is produced via reaction between propylene and sulfuric acid under heat in the presence of steam (Althaus et al., 2007).

Table 13 shows the material and energy flows for all intermediate materials.

Table 13: Material and energy flows for production of intermediate materials

Materials or Energy Sources	Intermediate Materials							
	$NaHCO_3$	$CoCO_3$	CH_2Cl_2	Terpineol	$MnCO_3$	8 Mol.% YSZ	3 Mol.% YSZ	Isopropanol
Material flows (ton/ton of product)								
Water	0.126							27.2
Sodium carbonate	0.741							
Carbon dioxide	0.309							
Cobalt sulfate		1.303						
Sodium bicarbonate		1.413			1.462			
Methane			0.189					
Chlorine			1.670					
Dichloromethane				0.551				
Liquid hydrogen				0.026				
Acetone				0.753				
Acetylene				0.338				
Manganese sulfate					1.314			
Yttria (yttrium oxide)						0.137	0.054	
Zirconia (zirconium oxide)						0.863	0.946	
Propylene								0.737
Sulfuric acid								0.175
Energy inputs (mmBtu/ton of product)								
Electricity	0.289			1.299				
Natural gas								0.859

REFERENCES

Alberola-Borràs, J.A., Baker, J.A., De Rossi, F., Vidal, R., Beynon, D., Hooper, K.E.A., Watson, T.M., Mora-Seró, I., 2018. Perovskite Photovoltaic Modules: Life Cycle Assessment of Pre-industrial Production Process. iScience 9, 542–551. https://doi.org/10.1016/J.ISCI.2018.10.020

Althaus, H.-J., Hischier, R., Osses, M., Primas, A., Hellweg, S., Jungbluth, N., Chudacoff, M., Chudacoff, Ö., 2007. Life Cycle Inventories of Chemicals - Data v2.0 (2007). Zurich.

Bareiß, K., de la Rua, C., Möckl, M., Hamacher, T., 2019. Life cycle assessment of hydrogen from proton exchange membrane water electrolysis in future energy systems. Appl. Energy 237, 862–872. https://doi.org/10.1016/J.APENERGY.2019.01.001

Bhandari, R., Trudewind, C.A., Zapp, P., 2014. Life cycle assessment of hydrogen production via electrolysis – a review. J. Clean. Prod. 85, 151–163. https://doi.org/10.1016/J.JCLEPRO.2013.07.048

Biganzoli, L., Racanella, G., Marras, R., Rigamonti, L., 2015. High temperature abatement of acid gases from waste incineration. Part II: Comparative life cycle assessment study. Waste Manag. 35, 127–134. https://doi.org/10.1016/J.WASMAN.2014.10.021

Cetinkaya, E., Dincer, I., Naterer, G.F., 2012. Life cycle assessment of various hydrogen production methods. Int. J. Hydrogen Energy 37, 2071–2080. https://doi.org/10.1016/J.IJHYDENE.2011.10.064

Donaldson, J.D., Beyersmann, D., 2005. Cobalt and Cobalt Compounds, in: Ullmann's Encyclopedia of Industrial Chemistry. John Wiley & Sons, Ltd, pp. 429–465. https://doi.org/10.1002/14356007.A07_281.PUB2

Frank, E.D., Elgowainy, A., Reddi, K., Bafana, A., 2021. Life-cycle analysis of greenhouse gas emissions from hydrogen delivery: A cost-guided analysis. Int. J. Hydrogen Energy 46, 22670–22683. https://doi.org/10.1016/J.IJHYDENE.2021.04.078

Gerloff, N., 2021a. Comparative Life-Cycle Assessment Analysis of Power-to-Methane Plants including Different Water Electrolysis Technologies and CO2Sources while Applying Various Energy Scenarios. ACS Sustain. Chem. Eng. 9, 10123–10141. https://doi.org/10.1021/ACSSUSCHEMENG.1C02002/ASSET/IMAGES/LARGE/SC1C02002_0024.JPEG

Gerloff, N., 2021b. Comparative Life-Cycle-Assessment analysis of three major water electrolysis technologies while applying various energy scenarios for a greener hydrogen production. J. Energy Storage 43, 102759. https://doi.org/10.1016/J.EST.2021.102759

Ghandehariun, S., Kumar, A., 2016. Life cycle assessment of wind-based hydrogen production in Western Canada. Int. J. Hydrogen Energy 41, 9696–9704. https://doi.org/10.1016/J.IJHYDENE.2016.04.077

Grigoriev, S.A., Fateev, V.N., Bessarabov, D.G., Millet, P., 2020. Current status, research trends, and challenges in water electrolysis science and technology. Int. J. Hydrogen Energy 45, 26036–26058. https://doi.org/10.1016/J.IJHYDENE.2020.03.109

Holst, M., Aschbrenner, S., Smolinka, T., Voglstätter, C., Grimm, G., 2021. Cost Forecast for Low Temperature Electrolysis - Technology Driven Bottom-Up Prognosis for PEM and Alkaline Water Electrolysis Systems. Freiburg.

IEA, 2019. The Future of Hydrogen.

IPCC, 2021. AR6 Climate Change 2021: The Physical Science Basis.

Mehmeti, A., Angelis-Dimakis, A., Arampatzis, G., McPhail, S.J., Ulgiati, S., 2018. Life Cycle Assessment and Water Footprint of Hydrogen Production Methods: From Conventional to Emerging Technologies. Environ. 5, 24. https://doi.org/10.3390/ENVIRONMENTS5020024

Norkem, 2022. Norkem [WWW Document]. URL https://www.norkem.com/products/manganese-carbonate (accessed 8.21.22).

Parvatker, A.G., Eckelman, M.J., 2020. Simulation-Based Estimates of Life Cycle Inventory Gate-to-Gate Process Energy Use for 151 Organic Chemical Syntheses. ACS Sustain. Chem. Eng. 8, 8519–8536. https://doi.org/10.1021/ACSSUSCHEMENG.0C00439/ASSET/IMAGES/LARGE/SC0C00439_0008.JPEG

Patyk, A., Bachmann, T.M., Brisse, A., 2013. Life cycle assessment of H2 generation with high temperature electrolysis. Int. J. Hydrogen Energy 38, 3865–3880. https://doi.org/10.1016/J.IJHYDENE.2013.01.063

Peng, L., Wei, Z., 2020. Catalyst Engineering for Electrochemical Energy Conversion from Water to Water: Water Electrolysis and the Hydrogen Fuel Cell. Engineering 6, 653–679. https://doi.org/10.1016/J.ENG.2019.07.028

Peterson, D., Vickers, J., Desantis, D., 2020a. Hydrogen Production Cost From PEM Electrolysis - 2019.

Peterson, D., Vickers, J., DeSantis, D., 2020b. Hydrogen Production Cost from High Temperature Electrolysis - 2020.

Ruth, M.F., Jadun, P., Elgowainy, A., Boardman, R., Gilroy, N., Connelly, E., Simon, A.J., Zuboy, J., 2021. The Technical and Economic Potential of Hydrogen within the United States. Golden, CO (United States). https://doi.org/10.2172/1086991

Strategic Analysis, 2022. Personal Communication with Strategic Analysis.

Vickers, J., Peterson, D., Randolph, K., 2020. Cost of Electrolytic Hydrogen Production with Existing Technology.

Wang, M., Elgowainy, A., Lee, U., Baek, K.H., Bafana, A., Benavides, P.T., Burnham, A., Cai, H., Cappello, V., Chen, P., Gan, Y., Gracida-Alvarez, U.R., Hawkins, T.R., Iyer, R.K., Kelly, J.C., Kim, T., Kumar, S., Kwon, H., Lee, K., Liu, X., Lu, Z., Masum, F.H., Ng, C., Ou, L., Reddi, K., Siddique, N., Sun, P., Vyawahare, P., Xu, H., Zaimes, G.G., 2022. Summary of Expansions and Updates in GREET® 2022 (No. ANL/ESIA-22/1). Argonne, IL (United States). https://doi.org/10.2172/1891644

Zhao, G., Kraglund, M.R., Frandsen, H.L., Wulff, A.C., Jensen, S.H., Chen, M., Graves, C.R., 2020. Life cycle assessment of H2O electrolysis technologies. Int. J. Hydrogen Energy 45, 23765–23781. https://doi.org/10.1016/J.IJHYDENE.2020.05.282

This page intentionally left blank.

Energy Systems and Infrastructure Analysis Division
Argonne National Laboratory
9700 South Cass Avenue, Bldg. 362
Lemont, IL 60439-4854

www.anl.gov